Polyhedron 246 (2023) 116669

Contents lists available at ScienceDirect

Polyhedron

journal homepage: www.elsevier.com/locate/poly

Synthesis and characterization of iron(II) Schiff-base complexes of tridentate mixed amine/imine ligands with *cis*- and *trans*-1,2-diaminocyclohexane backbones

Carl B. Hollandsworth [a,*], Blayne M. Griffin [a], John Raymon Pruden [a], Nikolay N. Gerasimchuk [b], Dustin E. Nevonen [c], Rachel R. Nickel [d], Johan van Lierop [d], Victor N. Nemykin [c,*]

[a] Lyon College, 2300 Highland Road, Batesville, AR, USA
[b] Missouri State University, Department of Chemistry, Temple Hall 456, Missouri State University, Springfield, MO, USA
[c] Department of Chemistry, University of Tennessee, 552 Buehler Hall, 1420 Circle Dr., Knoxville, TN, USA
[d] Department of Physics and Astronomy, University of Manitoba, 322 Allen Bldg., 30A Sifton Rd., Winnipeg, MB, Canada

ARTICLE INFO

Keywords:
Schiff-bases
Fe(II) complexes
Stereoisomers
Mössbauer spectroscopy
Electronic absorption spectroscopy
Solvatochromism in solutions
Electrochemical methods
X-ray analysis
DFT
TDDFT

ABSTRACT

The synthesis and characterization of two low-spin iron(II) complexes of tridentate mixed amine/imine Schiff bases is described. The complexes bear two tridentate ligands having either a *cis*- or *trans*-(1R,2R)-1,2-diaminocyclohexane backbone accompanied by a single pyridine-imino fragment. The complexes can be synthesized in protic solvents *via* ligand hydrolysis or by self-assembly. X-ray crystallography of the hexafluorophosphate salts is indicative that the tridentate ligands adopt a meridional configuration around the metal center. Synthesis using *trans*-(1R,2R)-diaminocyclohexane yields only one chiral stereoisomer of the iron complex. In the *cis*-1,2-diaminocyclohexane complex, the ligand amino groups form hydrogen-bonds to co-crystallized water, which in turn forms an extended hydrogen-bonding network with hexafluorophosphate counterions. The water molecule resides in a cavity formed from the two cyclohexyl backbones. The imine C═N stretch frequencies and long C═N bonds suggest a large degree of metal to ligand backbonding. Both complexes exhibit moderate solvatochromism. The circular dichroism (CD) spectrum of the enantiopure [*trans*-(1R,2R)-L_2Fe]$^{2+}$ cation has intense signals across the entire visible range. Mössbauer spectroscopy on the *cis*- complex confirms no noticeable spin-crossover behavior between 10 K and 300 K, as might be expected for a C_2-symmetrial coordination complex of iron(II) with a high degree of π-backbonding. Electrochemical experiments are indicative of one reversible oxidation wave which was assigned based on the spectroelectrochemical and theoretical data to the Fe^{II}/Fe^{III} couple. Density Functional Theory (DFT) calculations suggest that the HOMO in the *cis*- and *trans*- complexes is iron(II) centered, while the LUMO is delocalized over the organic ligands. Time-dependent density functional theory (TDDFT) confirms the presence of the numerous metal-to-ligand charge-transfer transitions between 380 and 620 nm.

1. Introduction

Iron(II) complexes are widely used in the stereospecific catalytic transformations of a large array of organic substrates [1]. The 1,2-diaminocyclohexane backbone can serve as a very simple and accessible motif for the preparation of bi-, tri-, and tetradentate chiral ligands which are potentially useful in chiral catalytic reactions. In particular, the isomeric diamines, *cis*- and *trans*-1,2-diaminocyclohexane, can undergo condensation with two equivalents of 2-pyridine carboxaldehyde to form double Schiff bases: achiral *cis*-(1R,2S)- and both chiral *trans*-(1R,2R) and *trans*-(1S,1S) enantiomers of N,N'-bis(pyridine-2-ylmethylene)-1,2-cyclohexanediamine (*cis*-**1** and *trans*-**1**; Scheme 1). *Cis*-**1** and the enantiomers of *trans*-**1** have been well characterized both structurally and spectroscopically [2–6].

The coordination chemistry of *trans*-1,2-diaminocyclohexane derivatives has been explored more than their corresponding *cis*- isomers [7]. This is due, in part, to the intrinsic optical activity of the *trans*-compounds which yield coordination complexes that can act as catalysts for asymmetric organic syntheses [8]. The coordination chemistry of the *meso* compound *cis*-**1** is not as well-explored. However, the *cis*-

* Corresponding authors at: Arkansas School for Math, Science, and the Arts, 200 Whittington, Ave., Hot Springs, AR, USA (C.B. Hollandsworth).
E-mail addresses: hollandsworthb@asmsa.org (C.B. Hollandsworth), vnemykin@utk.edu (V.N. Nemykin).

https://doi.org/10.1016/j.poly.2023.116669
Received 23 July 2023; Accepted 28 September 2023
Available online 12 October 2023

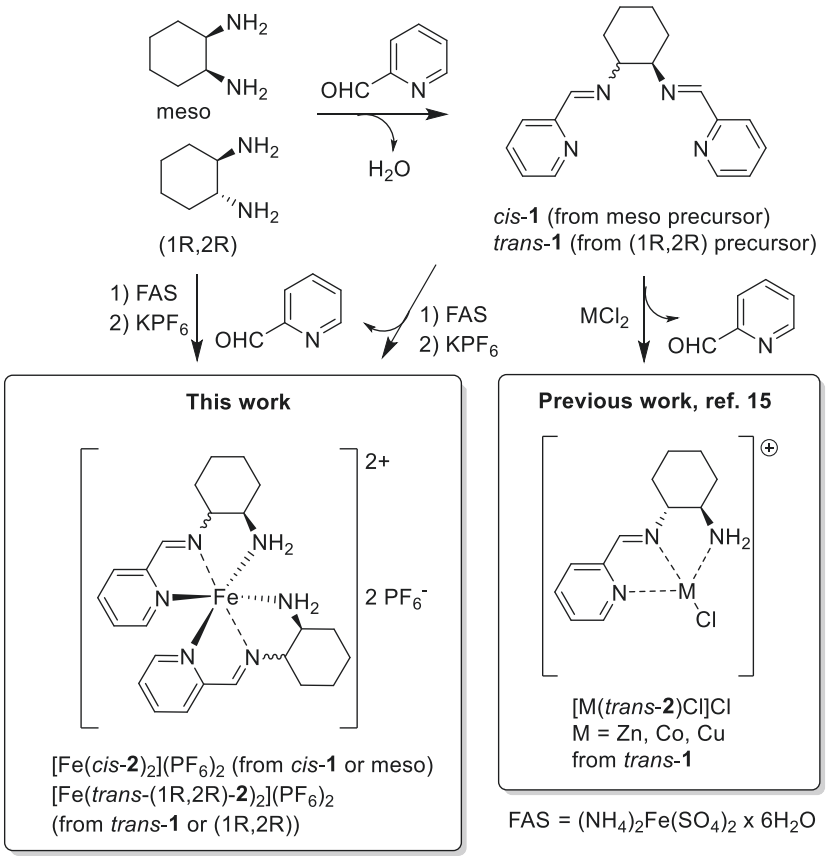

Scheme 1. Synthesis of [Fe(*cis*-**2**)$_2$](PF$_6$)$_2$ and [Fe(*trans*-(1R,2R)-**2**)$_2$](PF$_6$)$_2$.

arrangement of the imines in the ligand has been shown to give unique coordination geometries, particularly for lanthanide ions [9–14]. The current work is an exploration of coordination of such ligands to iron(II), which has been much less explored but has an interest for the asymmetric catalytic transformation of the organic substrates.

Upon reacting with Cu(II), Co(II), and Zn(II) chlorides in protic solvents, racemic *trans*-**1** undergoes a partial hydrolysis of one imine bond, losing one equivalent of 2-pyridinecarboxaldehyde, thus giving complexes of a mixed amine/imine tridentate ligand (*trans*- **2**) as shown in Scheme 1 [15]. Conversely, reactions in anhydrous, aprotic solvents yielded complexes in which *trans*-**1** acts as a tetradentate ligand. The Cu (II), Co(II), and Zn(II) chlorides of tridentate ligand **2** were not structurally characterized. It was postulated that the geometry around each M(II) center was *pseudo*-tetrahedral [15]. Luminescence studies on the paramagnetic complexes of *trans*-**1** with Cu(II) and Co(II) indicated reduced emission intensities at 395 nm and 440 nm respectively, when compared to the Zn(II) complex. Fluorescence bands were attributed to ligand-based ($\pi \rightarrow \pi^*$) transitions [5]. The coordination of this unique mixed amine-imine and tridentate ligand has not been explored for iron (II) complexes. Of particular interest is whether the coordination is four-coordinate or six-coordinate as is often the case for iron(II).

IR spectra of the complexes of *trans*-**2** showed N—H stretches in the 3200–3330 cm^{-1} range as well as azomethine C═N stretches assigned to transmissions at 1655, 1635, and 1639 cm^{-1} for Cu(II), Co(II), and Zn(II) respectively. The C═N stretch of the free ligand, *trans*-**2** occurs at 1643 cm^{-1}. Similar reactions between MCl$_2$ hydrates (where M = Co, Zn, Ni, and Cu) with bidentate benzylidene and cinnamalidene ligands also led to partial hydrolysis of the ligand in protic solvents to give complexes of a bidentate mixed amine/imine ligand [5]. Reactions of *cis*-**1** and those of divalent d[6] metals have not been explored. However, the self-assembly of an intensely-colored violet Fe(II) complex with two tridentate mixed amine/imine ligands similar to *cis*-**2** and *trans*-**2**, bridged with a 1,2-ethylene, rather than a 1,2-cyclohexyl, backbone has been described [16]. It is not clear if this intensely-colored complex showed solvatochromic behavior similar to the complexes described in this work.

In the present work, we describe the synthesis, structural, and spectroscopic characterization of the hexafluorophosphate salts of distorted octahedral, low-spin iron(II) complexes of C_2-symmetry having both *trans*- and *cis*-1,2-diaminocyclohexane backbones. These compounds, labelled herein as [Fe(*cis*-**2**)$_2$](PF$_6$)$_2$ and [Fe(*trans*-(1R,2R)-**2**)$_2$](PF$_6$)$_2$, can be formed by either monohydrolysis of *cis*-**1** or *trans*-**1** in the presence of Fe(II) and protic solvents or by self-assembly (Scheme 1). [Note that the "*cis*" and "trans" in [Fe(*cis*-**2**)$_2$](PF$_6$)$_2$ and [Fe(*trans*-(1R,2R)-**2**)$_2$](PF$_6$)$_2$ refer to the orientation of substituents on carbon atoms 1 and 2 of the cyclohexyl ring, not the stereochemistry of ligands around the metal center.] Similar self-assembly reactions with metal salts, aldehydes, and the other amines have been previously reported [17,18]. The complexes described here are intensely-colored and solvatochromic. There is also solid-state evidence that they can act as hydrogen-bond donors to water. It is our hope that these intensely-colored compounds might find applications as colorimetric indicators for small, hydrogen-bond accepting molecules.

2. Experimental details

2.1. Safety considerations

Dichloromethane, benzene, MeCN, and propionitrile are suspected carcinogens and should be used with appropriate ventilation and while wearing appropriate PPE. 2-pyridinecarboxaldehyde and 1,2-diaminocyclohexane should be treated as acute oral toxins. While we do not suspect that the novel ligand and iron(II) complexes synthesized in this work are acutely toxic, they have not been tested for toxicity and should

be treated accordingly.

2.2. Reagents and materials

95 % Ethanol (Flynn), dichloroethane (Spectrum), and hexanes (Flynn) were used as received without further purification. Deuterated MeCN (99 %-D) was used as received from Cambridge Isotope Labs. *cis*-1,2-Diaminocyclohexane (TCI, 98+%) and 2-pyridinecarboxaldehyde (TCI, 99+%) were used as received without further purification. Schiff bases *cis*-**1**, *trans*-**1**, and *trans*-(1R,2R)-**1** were prepared according to previously published syntheses [1]. Single crystals of *trans*-(1R,2R)-**1** were obtained as a benzene solvate, by slow evaporation of a saturated solution of the ligand in benzene over the course of several days. Tetrabutylammonium perchlorate (TBAP, for electrochemical analysis, ≥99.0 %) was purchased from Sigma Aldrich and recrystallized prior to use.

2.3. Synthesis of [Fe(cis-**2**)$_2$](PF$_6$)$_2$ and [Fe(trans-(1R,2R)-**2**)$_2$](PF$_6$)$_2$ via hydrolysis reaction

In a typical experiment, ammonium iron(II) sulfate hexahydrate (392 mg, 1.00 mmol) was added to 20.0 mL of 95 % EtOH in a 50 mL round bottom flask while stirring. The hexahydrate was completely dissolved after a period of several minutes by gently heating with an oil bath to 45 °C. A solution of *cis*-**1,** or *trans*-(1R,2R)-**1** (584 mg, 2.00 mmol) in 10.0 mL of EtOH was added giving an immediate color change to an intense indigo-colored solution. The reaction was allowed to stir for 2 h, after which the solvent was removed in a rotary evaporator under reduced pressure. The resulting dark blue solid was washed with CH_2Cl_2 (3 × 10 mL) to remove organic impurities, including the two equivalents of 2-pyridinecarboxaldehyde formed upon ligand hydrolysis. The loss of aldehyde was confirmed *via* IR of the residue remaining after evaporation of the CH_2Cl_2 wash ($\nu_{C=O} = 1713\ cm^{-1}$). The dark blue sulfate salt was then dissolved in a minimal amount of water and transferred to a separatory funnel. 20 mL CH_2Cl_2 was added, and the organic layer was discarded. Another 20 mL of CH_2Cl_2 was added along with 10 mL of saturated KPF_6 (aq). The blue color moved from the aqueous to the organic layer. The organic layer was washed two more times with saturated KPF_6 (aq) and the organic layers were combined and dried over anhydrous $MgSO_4$. The CH_2Cl_2 was removed under reduced pressure and the resulting blue solid was dried for 8 h at 50 °C under reduced pressure (50 torr). The hexafluorophosphate salts are hygroscopic but can be kept anhydrous by storing in a desiccator or under argon. The percent yields were as follows: [Fe(*cis*-**2**)$_2$](PF$_6$)$_2$ (46 %) and [Fe(*trans*-(1R,2R)-**2**)$_2$](PF$_6$)$_2$ (61 %).

2.4. Synthesis of Fe(II) complexes of [Fe(cis-**2**)$_2$](PF$_6$)$_2$ and [Fe(trans-(1R,2R)-**2**)$_2$](PF$_6$)$_2$ via self-assembly reaction

In a typical experiment, ammonium iron(II) sulfate hexahydrate (392 mg, 1.00 mmol) was dissolved in 5.0 mL of de-ionized water in a 50 mL round bottom flask, after which 15.0 mL of 95 % EtOH was added. 2-Pyridinecarboxaldehyde (214 mg, 2 mmol) was added in one portion while stirring. Subsequently, *cis*- or *trans*-(1R,2R)-1,2-diaminocyclohexane (228 mg, 2 mmol) was added dropwise with stirring, immediately giving an indigo-colored solution. The solution was allowed to stir at room temperature for 2 h, after which most of the ethanol and water were removed under reduced pressure. Further purification was achieved by extraction of the hexafluorophosphate salt into CH_2Cl_2 following a procedure identical to that of the hydrolysis route. Yields after crystallization from CH_2Cl_2: [Fe(*cis*-**2**)$_2$](PF$_6$)$_2$ (62 %), [Fe(*trans*-(1R,2R)-**2**)$_2$](PF$_6$)$_2$ (43 %). Characterization data for [Fe(*cis*-**2**)$_2$](PF$_6$)$_2$: The IR spectrum for {[Fe(*cis*-**2**)$_2$](PF$_6$)$_2$}·H$_2$O (Diamond ATR, ν in cm^{-1}) contains: 3652 and 3572 (asymmetric and symmetric O—H stretch of residual water), 3314 and 3259 (asymmetric and symmetric N—H stretch), 2951, 2863 (C—H stretching of cyclohexane ring), 1607 (C═N stretch), 826 (P-F stretch of anion) (Supporting Information Fig. S3). ^{1}H NMR (300 MHz, CD_3CN, ppm; atomic labels shown in Fig. S4): 10.0 (**H1**, s, *1H*), 8.10 (**H2**, d, $^1J_{H\text{-}H} = 7.9$ Hz, *1H*), 7.81 (**H3**, t, $^1J_{H\text{-}H} = 8.4$ Hz), 7.34 (**H5**, d, $^1J_{H\text{-}H} = 7.3$ Hz, *1H*), 7.13–7.15 (**H4**, m, *1H*), 5.07–5.10 (**H6**, m, *1H*), 2.68 (**H7**, m, 1H), 2.39 (**H8**, m, 1H), 1.52–1.66 (**H8′** and **H9-*H*11**, m, 7H) (Fig. S6**)**. The $^{13}C\{^1H\}$-NMR spectrum (75.6 MHz, CD_3CN, ppm relative to solvent ^{13}C peak at 118.3 ppm, carbon atom labeling scheme shown in Fig. S5**.** 167.1 (**C6**), 160.7 (**C5**), 154.0 (**C1**), 137.1 (**C4**), 127.5 (**C3**), 125.5 (***C2***), 68.0 (**C7**), 54.8 (**C12**), 29.5 (**C8**), 28.0 (**C11**), 23.5 (**C9/C10**), 17.5 (**C9/C10**) (Fig. S7). UV–Vis spectra (solvent, λ, nm; ε, $M^{-1}\ cm^{-1}$): DMSO 375 (3250), 510 (3480), 613 (8940); H_2O 368 (4620), 501 (5130), 598 (13,100); CH_3OH 368 (3040), 504 (3330), 602 (8300); acetone 368 (2710), 502 (3090), 598 (6430); CH_3CN 366 (3110), 499 (3570), 596 (9180); CH_2Cl_2 368 (1380), 497 (1520), 589 (3600) (Fig. S8) A sample of anhydrous [Fe(*cis*-**2**)$_2$](PF$_6$)$_2$ gave a negative reading on a magnetic susceptibility balance, indicating that the sample is diamagnetic. Elemental analysis: calculated for $C_{24}H_{34}F_{12}FeN_6P_2$: C – 38.31 %; H – 4.55 %; N – 11.17 %; found: C – 39.16 %; H – 4.55 %; N – 11.16 %. Characterization data for [Fe(*trans*-(1R,2R)-**2**)$_2$](PF$_6$)$_2$: The IR spectrum for [Fe(*trans*-(1R,2R)-**2**)$_2$](PF$_6$)$_2$ (Diamond ATR, ν in cm^{-1}) contains: 3325 and 3285 (asymmetrical and symmetrical N—H stretch), 2948, 2864 (C—H stretching of cyclohexane ring), 1604 (C═N stretch), 826 (P-F stretch of anion) (Fig. S9). The ^{1}H NMR (300 MHz, CD_3CN, ppm; atomic labels as shown in Fig. S4): 10.0 (**H1**, s, *1H*), 8.13 (**H2**, d, $^1J_{H\text{-}H} = 7.9$ Hz, *1H*), 7.83 (**H3**, t, $^1J_{H\text{-}H} = 8.4$ Hz), 7.31 (**H5**, d, $^1J_{H\text{-}H} = 7.3$ Hz, *1H*), 7.15–7.17 (**H4**, m, *1H*), 4.13 (**H6**, m, *1H*), 3.30 (**H7**, m, 1H), 2.39 (**H8**, m, 1H), 1.52–1.66 (**H8′** and **H9-*H*11**, m, 7H) (Figs. S10 and S11) The $^{13}C\{^1H\}$-NMR spectrum (75.6 MHz, CD_3CN, ppm relative to solvent ^{13}C peak at 118.3 ppm, peak labeling shown in Fig. S5. 164.8 (**C6**), 161.7 (**C5**), 154.5 (**C1**), 137.8 (**C4**), 128.6 (**C3**), 126.7 (***C2***), 72.3 (**C7**), 61.6 (**C12**), 34.4 (**C8**), 30.4 (**C11**), 25.0 (**C9/C10**), 24.8 (**C9/C10**) (Fig. S12). UV–Vis spectra (solvent, λ, nm; ε, $M^{-1}\ cm^{-1}$): DMSO 273 (15,876), 368 (5,965), 513 (2,443), 615 (6,241); H_2O 273 (10,206), 362 (3,044), 504 (1,776), 601(4,454); CH_2Cl_2 271 (11,188), 357 (3,263), 504 (741), 596 (4,857); CH_3OH 271 (16,445), 359 (6.170), 507 (2,411), 604 (6,200); CH_3CN 271 (15,931), 357 (6,163), 505 (2,634), 601 (6,961). UV–Vis spectra in different solvents can be found in Figs. S14 to S18. A sample of anhydrous [Fe(*trans*-(1R,2R)-**2**)$_2$](PF$_6$)$_2$ gave a negative reading on a magnetic susceptibility balance, indicating that the sample is diamagnetic. Moreover, both [Fe(*cis*-**2**)$_2$](PF$_6$)$_2$ and [Fe(*trans*-(1R,2R)-**2**)$_2$](PF$_6$)$_2$ afforded good quality NMR spectra without line broadening and shifts indicating a diamagnetic, low-spin nature of the Fe(II) centers at ambient temperature. Elemental analysis: calculated for $C_{24}H_{34}F_{12}FeN_6P_2$: C – 38.31 %; H – 4.55 %; N – 11.17 %; found: C – 38.84 %; H – 4.68 %; N – 10.91 %.

2.5. Physical methods

FTIR spectra were obtained on a Thermo Nicolet iS5 spectrophotometer and analyzed with OMNIC software (thermofisher.com). IR spectra were obtained on solid samples *via* ATR using a diamond transmission window. UV–Vis spectra were obtained using either a Thermo Genesys30, HP 8453, or Jasco-770 spectrophotometer. CD spectra were recorded using Jasco V-1500 spectropolarimeter. NMR spectra were recorded in deuterated MeCN on a 300 MHz JEOL ECX-300 FT at 298 K with chemical shifts referenced to signals from the deuterated solvent. Magnetic susceptibility measurements were performed on anhydrous solids of [Fe(*cis*-**2**)$_2$](PF$_6$)$_2$ and [Fe(*trans*-(1R,2R)-**2**)$_2$](PF$_6$)$_2$ using a Johnson-Matthey MSB Mk1 magnetic susceptibility balance. Elemental microanalysis was performed by Micro-Analysis, Inc. (Wilmington, DE).

2.6. X-ray analysis.

Single crystals of (E,E)-N,N'-(1R,2R)-1,2-cyclohexanediylbis[1-(2-pyridinyl)methanimine], *trans*-(1R,2R)-**1**, suitable for X-ray analysis

Table 1
Crystal and refinement data for *trans*-(1R,2R)-**1**, [Fe(*cis*-**2**)$_2$](PF$_6$)$_2$, and [Fe(*trans*-(1R,2R)-**2**)$_2$](PF$_6$)$_2$.

Parameter	Compound		
	trans-(1R,2R)-**1***	[Fe(*trans*-(1R,2R)-**2**)$_2$](PF$_6$)$_2$**	[Fe(*cis*-**2**)$_2$](PF$_6$)$_2$***
Empirical formula	$C_{18}H_{15}N_2$	$C_{25}H_{36}F_{12}FeN_6P_2Cl_2$	$C_{31}H_{49}F_{12}FeN_7OP_2$
Formula weight, g/M	277.88	837.284	855.30
Temperature, K	150(2)	120(2)	120(2)
Crystal system	trigonal	monoclinic	monoclinic
Color /habitus	colorless block	black-red plate	dark-red block
Crystal size (mm)	0.224 × 0.414 × 0.523	0.099 × 0.162 × 0.215	0.125 × 0.167 × 0.232
Space group	$P3_121$, #152	$P2_1$, #4	$P2_1/c$, #14
a	8.9657(6)	9.147(5)	18.0283(13)
b	8.9657(6)	18.314(9)	11.3779(9)
c	22.5883(14)	10.084(5)	16.5513(12)
α	90	90	90
β	90	92.230(5)	94.581(1)
γ	120	90	90
Volume (Å^3)	1572.47(18)	1688.0 (14)	3384.2(4)
Z	4	2	4
ρ_{calc} (g/cm^3)	1.1737	1.647	1.679
μ (mm^{-1})	0.071	0.795	0.797
F(000)	594	854	1744
2θ range for data (°)	5.24 to 65.06	4.04 to 51	4.24 to 52.88
Index ranges:	$-13 < h < 13$ $13 < k < 13$ $33 < l < 34$	$-11 < h < 11$ $23 < k < 23$ $12 < l < 12$	$22 < h < 22$ $14 < k < 14$ $-20 < l < 20$
Reflections collected	27,417	20,807	41,099
Independent	3698 [Rint = 0.0354, Rσ = 0.0242]	6271 [Rint = 0.0786, Rσ = 0.1102]	6956 [R(int) = 0.0534, Rσ = 0.0712]
Data/restrains/parameters	3698 / 0 / 180	6271 / 61 / 433	6956 / 228 / 514
Goodness-of-fit on F^2	1.049	1.046	1.027
Final R indices:	1883 [I > 2σ(I)]; R1 = 0.0379 w$R2$ = 0.0988	6271 [I > 2σ(I)]; R1 = 0.0656 w$R2$ = 0.1694	5088 [I > 2σ(I)]; R1 = 0.0437 w$R2$ = 0.0961
All data:	R1 = 0.0451; w$R2$ = 0.1028	R1 = 0.0937; w$R2$ = 0.1883	R1 = 0.0696; w$R2$ = 0.1063
Peak/hole difference, e (A^{-3})	+0.31 / −0.21	+0.81 / −1.12	+0.636 / −0.447
Flack parameter	−0.9(10)	−0.01(3)	n/a
Volume taken, A^3 (%)	963.7 (61.3)	1068.7 (63.3)	2257.8 (66.7)

* - benzene solvate; **- CH_2Cl_2 solvate; ***- water and CH_2Cl_2 solvate.

were obtained as colorless blocks after slow evaporation of a saturated solution of the compound in benzene (Fig. S16). Dark red blocks of complex [Fe(*cis*-**2**)$_2$](PF$_6$)$_2$ monohydrate dichloromethane solvate, suitable for X-ray analysis, were grown by allowing a concentrated solution of the hydrated complex in CH_2Cl_2 to cool at 5 °C over the course of 1 week. Single crystals of [Fe(*trans*-(1R,2R)-**2**)$_2$](PF$_6$)$_2$ dichloromethane solvate were obtained from a concentrated solution in CH_2Cl_2 upon standing at room temperature overnight (Fig. S17).

Suitable single crystals were inspected, selected, and handled in NVH oil, with subsequent mounting on a thin glass fiber, or placed into a CryoLoop and then attached to a copper pin positioned on the goniometer head of a diffractometer equipped with a CCD area detector. All

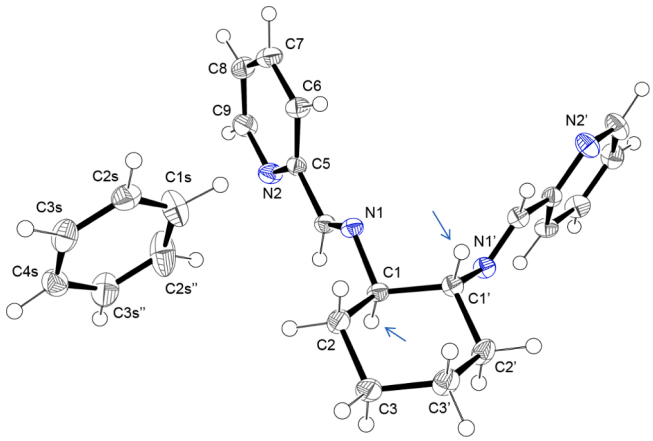

Fig. 1. Molecular structure and numbering scheme for principal atoms in *trans*-(1R,2R)-**1**, stoichiometric benzene solvate (shown as GROW option). Arrows indicate *trans*-orientations of H-atoms. Symmetry operations for atomic symbols with prime notations ‘: −y; −x−y; z + 1/3; and for “: −x + y; −x; z + 2/3.

data sets were measured at low temperatures as specified in the crystal structure and refinement data in Table 1. Data were collected in ω scan mode using the Mo tube (Kα radiation; λ = 0.71073 Å) with a highly oriented graphite monochromator. The intensities for the latter radiation were integrated from four series of 364 exposures each, covering 0.5° in ω, with the total data set being a sphere. The space group determination was done with the aid of XPREP software [19]. The absorption correction was performed using values from face-indexed crystals and numerical values obtained from the set of images recorded with a video-microscope, followed by the SADABS program that was included in the Bruker AXS software package [20,21].

All structures were solved by direct methods, and refined by least squares on weighted F^2 values for all reflections using SHELXS-2013. The structures reported herein are well refined and without apparent errors. All hydrogen atoms in the structures presented were found on the electron density map and refined objectively. The crystal structures and packing diagrams were drawn using the ORTEP 3v2 [22,23] and Mercury software packages [24]. Thermal ellipsoids appearing in figures are drawn at their 50 % probability level.

2.7. Thermal analysis.

The TG analysis for [Fe(*cis*-**2**)$_2$](PF$_6$)$_2$ was performed on a TA Instrument Q-600 (Delaware, USA) in an alumina crucible in the range between 30 and 1000 °C under nitrogen flow at 100 ± 1 mL/min and a heating rate of 10 °C/min. The crucible was calcined prior to each experiment using a propane torch. Data of the TG analyses were processed using the TA Universal Analysis software package. Details are presented in Figs. S18-S21.

2.8. Mössbauer spectroscopy.

Mössbauer spectra were obtained at either room temperature or 10 K. The Mössbauer spectroscopy experiments were collected using zero field in a transmission geometry using WissE1 constant acceleration drive and a 10 GBq Cobalt-57-in-Rh source. A Janis SHI-850 closed-cycle refrigerator was used to collect the low temperature spectra. The calibration of all spectra was performed relative to α-Fe at room temperature. The Mössbauer spectra were fit using a nonlinear least squares analysis where each iron-site was characterized by an isomer shift with energies set by the appropriate nuclear transitions while using a Lorentzian line shape doublet. The data analyses were performed using in-house produced codes.

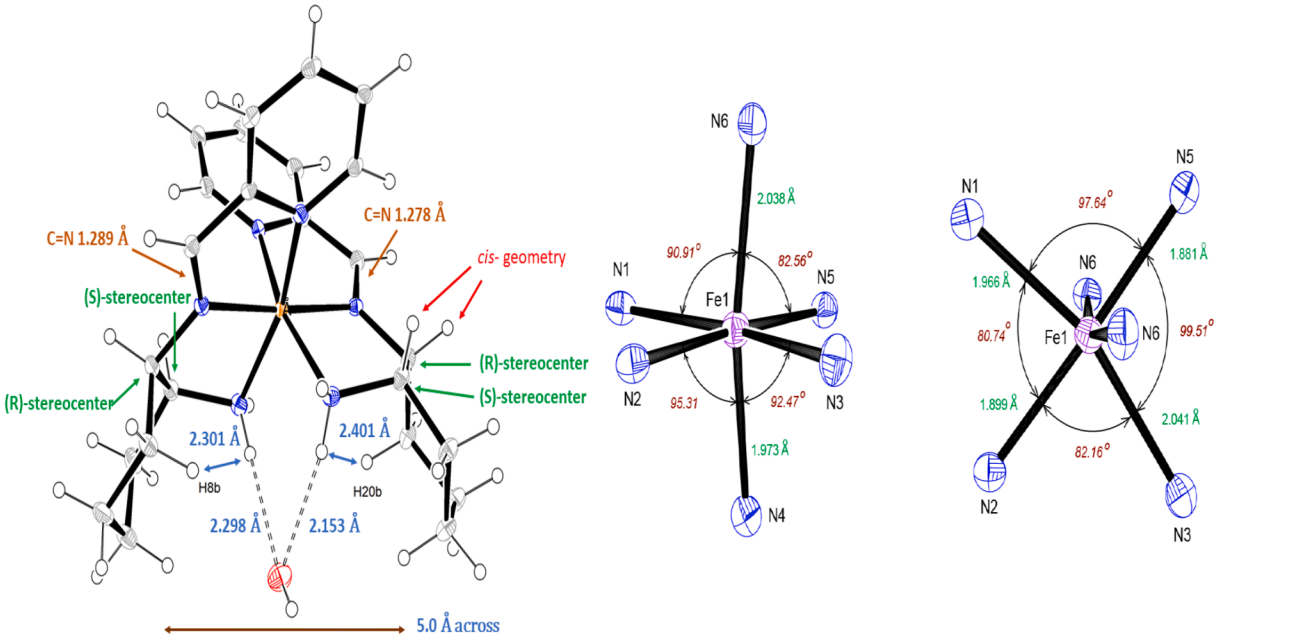

Fig. 2. Left: An ORTEP drawing of the fragment of the crystal structure of the Fe(II) cation in [Fe(*cis*-**2**)$_2$](PF$_6$)$_2$ showing a co-crystallized water molecule. The imine C═N bond distances and NH$_2$ to H$_2$O hydrogen bonding distances are indicated, along with stereochemical configurations of the substituted cyclohexyl carbon atoms. Short N—H—C—H distances between coordinated amino- and cyclohexyl-groups are shown. Color key: iron (orange), oxygen (red), nitrogen (blue), carbon (grey), hydrogen (white). Right: Geometry of the Fe center in the structure of [Fe(*cis*-**2**)$_2$](PF$_6$)$_2$: two orthogonal views showing principal bond lengths and valence angles in the Fe(II) polyhedron. The axial *N*-donor atoms tilt angle: <N4-Fe1-N6 = 163.59°. Other angles: N2-Fe1-N6 = 101.06°; N3-Fe1-N6 = 90.98°; N1-Fe1-N4 = 90.51°; N5-Fe1-N4 = 81.05°.

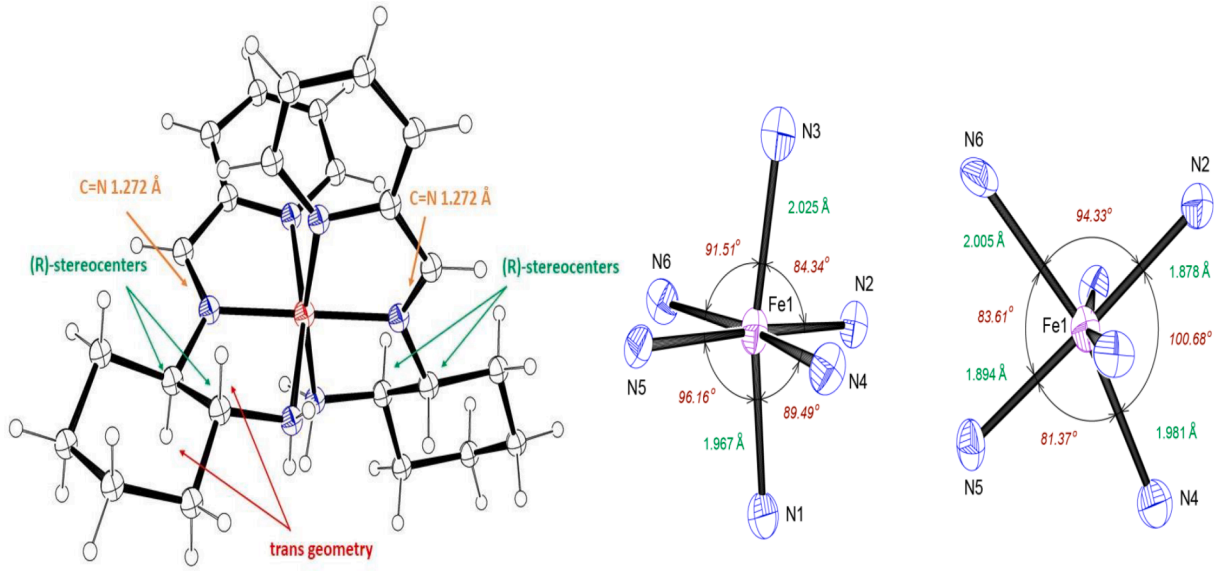

Fig. 3. Left: An ORTEP drawing of the Fe(II) complex ion of [Fe(*trans*-(1R,2R)-**2**)$_2$](PF$_6$)$_2$C = N bond distances and stereochemical configurations are shown. Key: iron (red), nitrogen (blue), carbon (white ellipsoid), hydrogen (white sphere). Right: Environment of Fe center in the structure of [Fe(*trans*-(1R,2R)-**2**)$_2$](PF$_6$)$_2$: two orthogonal views showing principal bond lengths and valence angles in Fe(II) polyhedron. The axial *N*-donor atoms tilt angle < N3-Fe1-N1 = 165.67°. Other angles: N5-Fe1-N3 = 98.28°; N4-Fe1-N3 = 81.30°; N6-Fe1-N1 = 92.36°; N2-Fe1-N1 = 81.30°.

2.9. Electrochemical and spectroelectrochemical measurements.

Electrochemical data were collected using a CH-620 analyzer with platinum working, platinum auxiliary, and Ag/AgCl pseudo-reference electrodes. Ferrocene was used as an internal standard for the studied compounds and the reported potentials were corrected to the Fc/Fc$^+$ couple. All electrochemical experiments were conducted in a MeCN/0.1 M tetrabutylammonium perchlorate (TBAP) system. The spectroelectrochemical experiments were performed using a Jasco V-770 EA spectrophotometer in tandem with a CH Instruments CH-620 electrochemical analyzer which was operated using the bulk electrolysis mode. The data were collected using a custom-made 1 mm cell, a platinum mesh working electrode, platinum auxiliary electrode, Ag/AgCl pseudo-reference electrode, and a 0.3 M solution of TBAP in MeCN. In addition, tThe Fe compounds studied were oxidized using 1–2.5 μL of nitrosonium tetrafluoroborate in MeCN (0.023 M). These oxidations were monitored *via* UV–Vis spectra on a Jasco V-770 spectrophotometer.

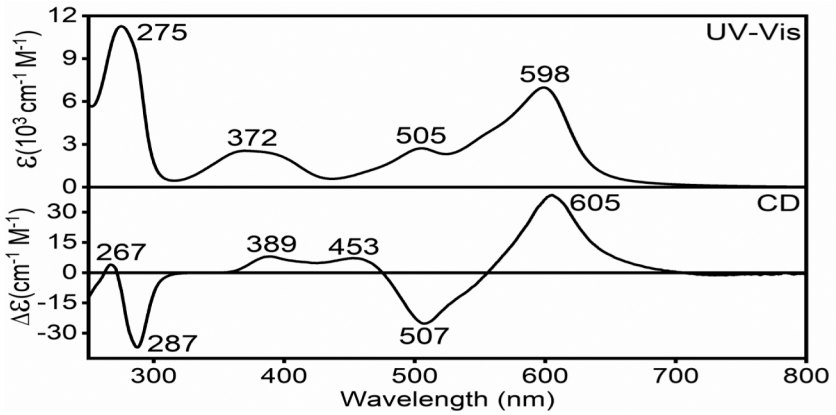

Fig. 4. UV–Vis and CD spectra of enantiopure [Fe(*trans*-(1R,2R)-**2**)$_2$](PF$_6$)$_2$ in MeCN.

Table 2
The most intense peaks (nm) and molar absorptivity constants (M^{-1} cm^{-1}) in the visible spectrum in different solvents.

[Fe(*cis*-**2**)$_2$](PF$_6$)$_2$	
H_2O	598 (13,100), 501 (5,130), 368 (4,620)
CH_2Cl_2	589 (3,600), 497 (1,520), 368 (1,380)
MeCN	596 (9,180), 499 (3,570), 366 (3,110)
DMSO	613 (8,940), 510 (3,480), 375 (3,250)
CH_3OH	602 (8,300), 504 (3,300), 368 (3,040)
acetone	598 (6,430), 502 (3,090), 368 (2,710)
[Fe(*trans*-(1R,2R)-**2**)$_2$](PF$_6$)$_2$	
H_2O	601 (4,450), 504 (1,780), 362 (3,040)
CH_2Cl_2	596 (4,860), 504 (3,740), 357 (3,260)
MeCN	598 (6,960), 505 (2,630), 357 (6,160)
DMSO	615 (6,240), 513 (2,440), 368 (5,970)
CH_3OH	604 (6,200), 507 (2,410), 359 (6,170)

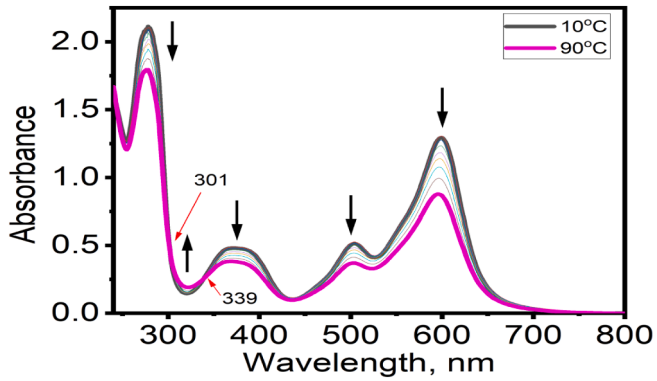

Fig. 5. Series of overlaid UV–Vis spectra of [Fe(*cis*-**2**)$_2$](PF$_6$)$_2$ in propionitrile recorded at different temperatures in 1 cm quartz cuvette. Two isosbestic points are indicated with green arrows.

Table 3
Experimental and simulated Mössbauer fitting parameters for [Fe(*cis*-**2**)$_2$](PF$_6$)$_2$.

Complex	*Conditions*	*δ, (mm/s)*	*ΔEQ, (mm/s)*
[Fe(*cis*-**2**)$_2$](PF$_6$)$_2$	Exp. 10 K (ℓ)*	0.308	0.914
[Fe(*cis*-**2**)$_2$](PF$_6$)$_2$	Exp. 10 K (s)*	0.309	0.961
[Fe(*cis*-**2**)$_2$](PF$_6$)$_2$	Exp. 300 K (s)	0.240	0.966
[Fe(*cis*-**2**)$_2$](PF$_6$)$_2$	DFT/RevTPSS	0.270	−0.913
{[Fe(*cis*-**2**)$_2$](PF$_6$)$_2$}***H$_2$O**	DFT/RevTPSS	0.272	−0.867

*ℓ = frozen solution; s = solid.

2.10. Computational details

All calculations were run using Gaussian 16 [25]. BP86 [26,27] with Wachters' full-electron basis set [28] (Wf) for iron and the 6-311G(d) basis set [29] for all other atoms were used for all geometry optimizations. Vibrational frequencies were calculated to ensure all geometries were local minima. Time-dependent density functional theory (TDDFT) with revTPSS [30,31] was used to calculate the first 60 excited states of each molecule. In addition, the B3LYP [32], BP86 [32], HFS [33–35], M11L [36], MN15L [37], O3LYP [38], OLYP [39], PBE [40,41], SOGGA11 [42], SVWN5 [43], tHCTH [44], tHCTHhyb [45], TPSS [46], TPSSh [45,46], VSXC [47], and wB97D [48] functionals were tested on a single compound because of the well-known exchange correlation functional dependance on the calculated vertical excitation energies in iron complexes [49,50]. The same basis sets used for the geometry optimizations were also used for the TDDFT calculations. Single point calculations using the same parameters as the TDDFT calculations were also performed. All calculations were run in solution using the PCM model [51], with dichloromethane (DCM) as the solvent. QMForge [52] was used for the molecular orbital composition analyses.

3. Results and discussion

3.1. Synthesis

Compounds [Fe(*cis*-**2**)$_2$](PF$_6$)$_2$ and [Fe(*trans*-(1R,2R)-**2**)$_2$](PF$_6$)$_2$ were synthesized in good yields by either self-assembly (iron(II) salt, two equivalents of pyridine carboxaldehyde, two equivalents of 1,2-diaminocyclohexane, two equivalents of KPF$_6$) or hydrolysis of two equivalents of *cis*-**1** or *trans*-**1** in the presence of ammonium iron(II) sulfate. Full discussion of the syntheses and routine spectroscopic measurements are found in the supplemental information.

The The *cis*- and *trans*- "tetradentate" bis-imine starting materials have C═N stretches in the IR spectra at 1640 and 1637 cm^{-1} respectively.[2] In the Fe(II) complexes, the C═N stretch frequency is reduced to 1605 and 1607 cm^{-1} respectively. We interpret this as a weakened C═N bonding due Fe(II) backbonding into the C═N π* molecular orbital. The imino N═C-**H** resonances in the ^{1}H NMR spectra are found at 8.31 and 8.20 ppm for the trans- and cis- tetradentate ligands, respectively.[2] These resonances shift to lower field, at almost exactly 10.0 ppm for both metal complexes. Back donation from the d-orbitals to the π* molecular orbital removes electron density from the C═N and leads to deshielding relative to the neutral ligand. The same trend is seen for the imino ^{13}C resonances. In the bis-imines, the resonance is found at around 161 ppm for both the *cis*- and *trans*- ligands.[2] The imino ^{13}C resonance shifts slightly to 165 and 168 ppm in the metal complexes. This serves as further spectroscopic evidence that the C═N π bond density is reduced by backbonding from the Fe ion.

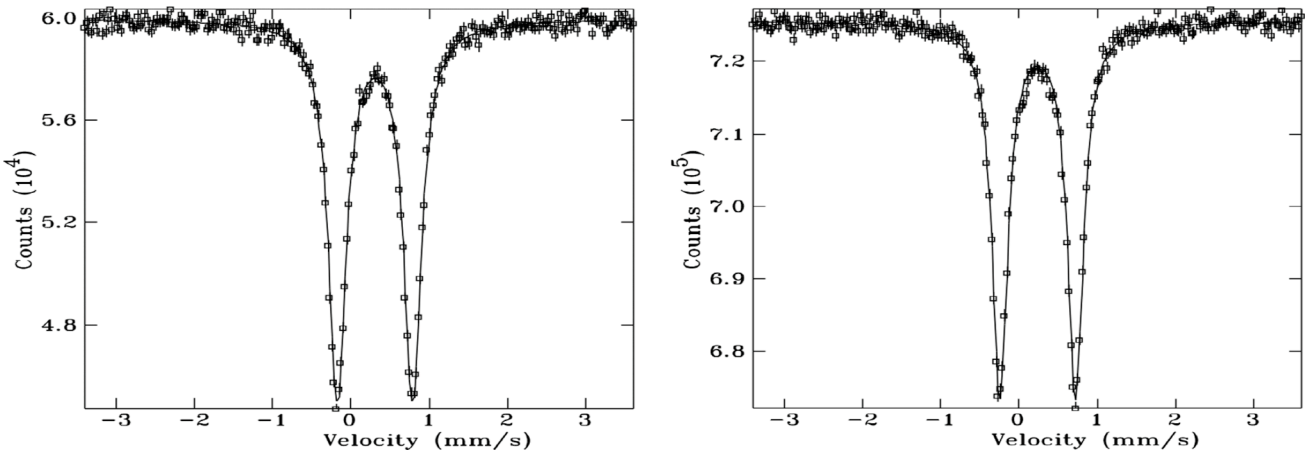

Fig. 6. The ^{57}Fe Mossbauer Spectra of [Fe(*cis*-**2**)$_2$](PF$_6$)$_2$ at 10 K (left) and 300 K (right) showing no temperature dependence of the quadrupole splitting, which is typical of a stable, non-SCO low-spin iron(II) complex.

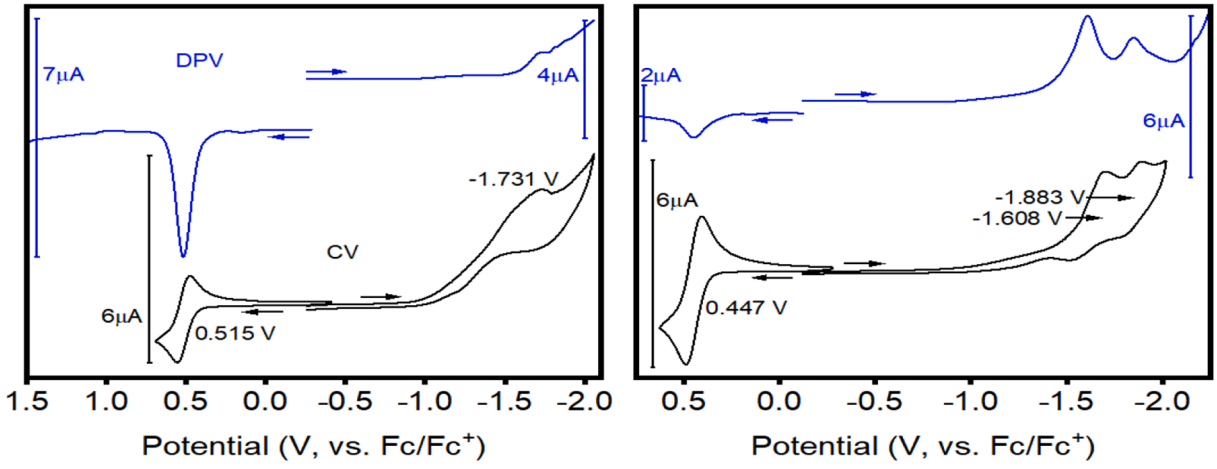

Fig. 7. CV (black) and DPV (blue) voltammograms for [Fe(*cis*-**2**)$_2$](PF$_6$)$_2$ (left) and [Fe(*trans*-(1R,2R)-**2**)$_2$](PF$_6$)$_2$ (right) using a 0.1 M TBAP/MeCN system.

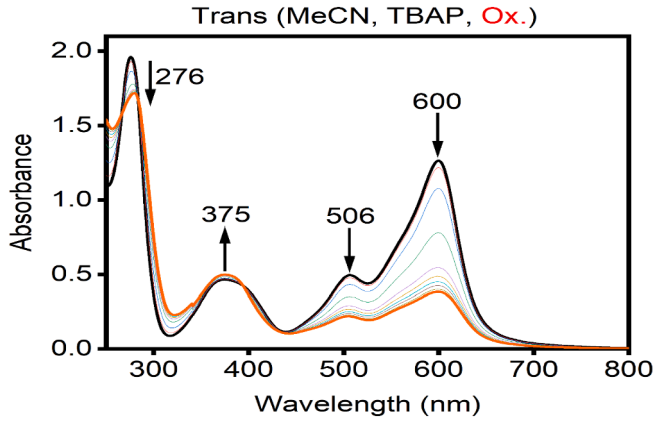

Fig. 8. Spectroelectrochemical oxidation of [Fe(*trans*-(1R,2R)-**2**)$_2$](PF$_6$)$_2$ using a 0.3 M TBAP/MeCN system.

3.2. Crystal structures

Slow evaporation of solvent from a concentrated solution of *trans*-(R,R)-**1** in benzene resulted in the isolation of colorless crystals of the ligand as benzene solvate. It was characterized by X-ray analysis (Table 1 and Fig. 1), This Schiff-base bearing two imine functionalities crystallized in a very rare (for organic compounds) trigonal, non-centrosymmetric P3$_1$21 (#152) space group. Benzene molecules occupy channels in the structure running along the *a*-direction (Fig. S22-S25).

In the crystal structures of both [Fe(*cis*-**2**)$_2$](PF$_6$)$_2$ and [Fe(*trans*-(1R,2R)-**2**)$_2$](PF$_6$)$_2$, the Fe(II) ion shows complexation of two tridentate mixed imine/amine ligands. The ligands orient in a meridional configuration around the iron center with distorted octahedral coordination of the metal (Figs. 2 and 3). The neutral tridentate ligands form two five-membered chelate rings each with very close "bite angles" ranging from 80.71° to 82.76°. In [Fe(*cis*-**2**)$_2$](PF$_6$)$_2$, the imine nitrogen atoms of the two different ligands are found *trans* to each other with an almost linear bond angle of 176.0°, and with the two shortest metal-nitrogen bond distances of 1.899 and 1.881 Å for the Fe1-N5 and Fe1-N2 pair, respectively (1.89 Å average length). The shortness of these two bonds suggests a strong metal-to-ligand backbonding interaction with the imine nitrogen atom (Fig. 2). Likewise, the C═N bond distances are elongated relative to those in the *cis*-**1** and *trans*-(1R,2R)-**1** Schiff base structures. For [Fe(*cis*-**2**)$_2$](PF$_6$)$_2$, The C═N distances are 1.278 and 1.289 Å, whereas those in the crystal structure of the Schiff base *cis*-**1** are 1.267 and 1.264 Å.[2] The C═N stretching frequency for *cis*-**1** is found at a typical value of 1637 cm^{-1}. The C═N stretches in the IR spectra of [Fe(*cis*-**2**)$_2$](PF$_6$)$_2$ and [Fe(*trans*-(1R,2R)-**2**)$_2$](PF$_6$) occur at 1607 and 1604 cm^{-1}, respectively. The shortness of the C═N bonds in the Fe complexes, taken together with the lower energy stretching frequency, is further evidence of significant metal-to-ligand backbonding.

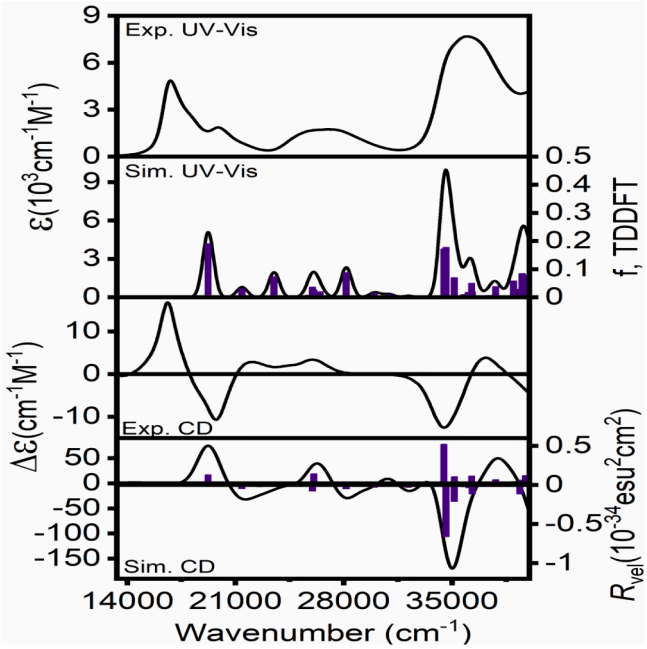

Fig. 9. Experimental (DCM) TDDFT-PCM (DCM) predicted UV–Vis and CD spectra of [Fe(*trans*-(1R,2R)-**2**)$_2$]$^{2+}$.

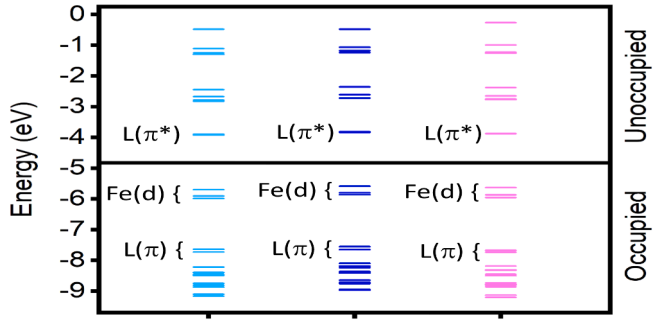

Fig. 10. DFT-predicted energy-level diagram for [Fe(*cis*-**2**)$_2$]$^{2+}$ (left), {[Fe(*cis*-**2**)$_2$]*H_2O}$^{2+}$ (center), and [Fe(*trans*-(1R,2R)-**2**)$_2$]$^{2+}$ (right).

In the structure of [Fe(*cis*-**2**)$_2$](PF$_6$)$_2$, the next Fe-N bond distance in length (slightly longer bond distance) is a pair of Fe-N$_{pyridine}$ bonds Fe1-N1 = 1.966 Å and Fe1-N4 = 1.973 Å. The pyridine groups are in *cis*-positions relative to each other around the metal center (Fig. 2). The average bond length here is 1.97 Å, which is 0.08 Å longer on average than in the previous pair of metal-nitrogen bonds above. Lastly, the third pair of longest bonds (Fe1-N3 = 2.041 Å and Fe1-N6 = 2.038 Å) of the amino-groups has an average length of 2.04 Å. This is 0.07 Å longer than the same for the second pair of bonds and 0.15 Å longer than the shortest ones discussed above.

The polyhedron coordination structure of the low-spin Fe(II) center represents a highly distorted (in lengths) octahedron in which four atoms (N2, N4, N5, and N6) of one Schiff base and Fe form a planar arrangement including the pyridine group with the N4 atom (Fig. 2). The second Schiff base with N1-N3 atoms is perpendicular to the above plane, resulting in a meridional arrangement of the two tridentate ligands. The meridional relationship of the tridentate ligands gives rise to the methylene –(CH$_2$)$_4$ bridges of the *cis*-1,2-diaminocyclohexyl rings, each in chair conformation, pointing towards the same general region of space. The rings create a cavity in which the water molecule is located and hydrogen-bonded to the nitrogen of the amino group on the ligand. The extra annular rim of the cavity is roughly 5 Å across, reminiscent of those found for calixarenes. This is a much smaller extra annular distance than those calculated for iron(III) phenolic calix[4]arenes having no bound molecules within the host cavity [53]. The oxygen atom of the water molecule is hydrogen-bonded to both amine-group hydrogens at distances of 2.198 and 2.253 Å. Two of the axial hydrogen atoms on the cyclohexyl carbons adjacent to the imine-substituent, point directly into the cavity in the direction of the water molecule (labeled H8b and H20b in Fig. 2).

One feature of the extended structure of [Fe(*cis*-**2**)$_2$](PF$_6$)$_2$ is hydrogen bonding between the co-crystallized water molecule, ligand amino groups, and hexafluorophosphate counterions. There are also short N—H—Cl(solvent) and C—H—F(anion) electrostatic contacts, the geometry of which is present in Figs. S26–S29. Further, the X-ray crystal structure data shows that [Fe(*cis*-**2**)$_2$](PF$_6$)$_2$ packs in alternating methylene chloride, [PF$_6$]$^-$, and Fe(II) complex ••• [PF$_6$]$^-$ layers (Fig. S29). The forces of close contact between particles include five hydrogen-bonding interactions: the hydrogen atoms of the water molecule bridge its oxygen atom with fluorine atoms on each of the two counter ions (bond distances of 2.130 and 2.245 Å), whereas one hydrogen atom on each of the two ligand NH$_2$ groups bridge amine nitrogen atoms and the oxygen atom of the water molecule (bond distances of 2.153 and 2.298 Å). A different hydrogen atom on one of the amine groups interacts with fluorine of hexafluorophosphate at a much longer distance of 2.682 Å (Fig. S29), Although long, this distance is still within an acceptable range to consider it a hydrogen-bonding interaction [54].

The crystal structure of the [Fe(*trans*-(1R,2R)-**2**)$_2$](PF$_6$)$_2$ complex contains no disordered fragments and an explanation for the assignment of stereocenters on the Schiff base is presented in Fig. 3. Two neutral tridentate ligands in this complex also form two five-membered chelate rings with values of their "bite angles" from 81.30° to 84.34°. These are slightly bigger than in the case of the structure of [Fe(*cis*-**2**)$_2$](PF$_6$)$_2$ reflecting increased steric demand for the [Fe(*trans*-(1R,2R)-**2**)$_2$](PF$_6$)$_2$ complex. The imine nitrogen atoms of the two different ligands are found *trans* to each other with an almost linear bond angle of 176.69°. Again, they form the two shortest metal-nitrogen bond distances of 1.878 and 1.894 Å in Fe1-N2 and Fe1-N5 pair (1.886 Å average length). Similar to the [Fe(*cis*-**2**)$_2$](PF$_6$)$_2$ complex, the next in length is a pair of Fe-N(py group) bonds Fe1-N1 = 1.967 Å and Fe1-N4 = 1.981 Å being in *cis*-position to each other about the metal center (Fig. 3). The average bond length here is 1.974 Å. which is 0.088 Å longer in average than in the previous pair of metal-nitrogen bonds above. Finally, the shortest pair of Fe-N bonds is between the metal center and amino-groups: Fe1-N3 = 2.025 Å and Fe1-N6 = 2.005 Å (average is 2.015 Å). This is 0.041 Å longer than the same for the second pair of bonds, and 0.129 Å longer than the shortest ones presented above. Again, those two Fe-amino-group bonds are in a *cis*-position to each other relative to the metal center (Fig. 3). The coordination polyhedron of the low-spin Fe-center represents a highly rhombically-distorted octahedron in which there is a strong "squeeze" of the metal ion by two opposite imine nitrogen atoms followed by the *cis*-oriented *N*-atoms of the heterocycle (Fig. 3). Those four (shorter than 2 Å) bonds are responsible for adoption by the metal center's low-spin ground state which was confirmed by Mössbauer spectroscopy. Contrary to the structure of [Fe(*cis*-**2**)$_2$](PF$_6$)$_2$ described above, there is no H-bonding between the Fe(II) cationic center and anions in the structure of the *trans*-analogue. However, there are important short intramolecular electrostatic contacts (N—H—F and C—H—F) that provide close-packing in the structure (Figs. S30-S33). The crystal packing nature of [Fe(*trans*-(1R,2R)-**2**)$_2$](PF$_6$)$_2$ molecules is primarily a result of van-der-Waals contacts while CH$_2$Cl$_2$ solvent molecules occupy channels along the *a*-direction.

3.3. Spectroscopy

The UV–Vis of the Fe-complexes demonstrated several consistent and intense peaks belonging to π-π * transitions in the ligands, as well as the most intense metal-to-ligand charge-transfer (MLCT) band at ~ 600 nm, which is responsible for the compounds' dark-blue appearance in

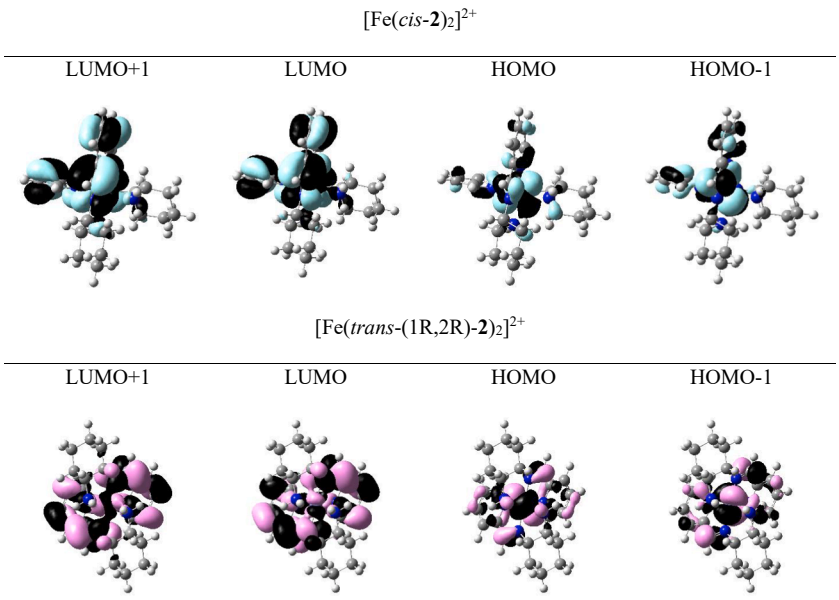

Fig. 11. DFT-predicted frontier molecular orbitals for $[Fe(cis\text{-}\mathbf{2})_2]^{2+}$ and $[Fe(trans\text{-}(1R,2R)\text{-}\mathbf{2})_2]^{2+}$.

solution. In addition, an intense band around 300 nm was also observed. The exact positions of the transitions were determined by full line-shape analysis of the spectroscopic envelopes (Fig. 4 and Figs. S35-S36). Both the cis- and trans- complexes exhibit pronounced solvatochromic behavior in solvents of different polarity with the largest difference of 665 cm^{-1} (0.07 eV) observed for the low-energy transition at ~ 600 nm between the CH_2Cl_2 and DMSO solutions (Table 2). Transition energies for the most intense peak range from 16,978 cm^{-1} in dichloromethane to 16,313 cm^{-1} in the more polar DMSO (Fig. S37). The most polar solvent, H_2O, possesses an intermediate transition energy for the most intense peak of 16,722 cm^{-1}. The molar extinction coefficient for the most intense peak located around 600 nm ranges in intensity from 13,100 M^{-1} cm^{-1} in water to 3,600 M^{-1} cm^{-1} in CH_2Cl_2 (Table 2). These peak intensities follow the same trend for the other two transitions. Linear correlations between the molar extinction coefficients for the low-energy band and dielectric constant of the solvent have been established (Fig. S40).

The circular dichroism (CD) spectrum of the enantiopure $[Fe(trans\text{-}(1R,2R)\text{-}\mathbf{2})_2](PF_6)_2$ is shown in Fig. 4. It is dominated by two strong signals at 606 nm and 507 nm and one strong signal observed at 287 nm. The lowest-energy band at 605 nm has a positive amplitude, while those at 507 and 287 nm have negative amplitudes. In addition, several overlapping low-intensity transitions between 300 and 500 nm were observed in the CD spectrum of this compound. The energies of 605, 507, and 287 nm bands observed in CD spectra of $[Fe(trans\text{-}(1R,2R)\text{-}\mathbf{2})_2](PF_6)_2$ correlate well with the absorption bands observed at 598, 505, and 275 nm in the UV–Vis spectrum of this complex (Fig. 4). Both the positive and negative amplitude bands at 605 and 505 nm are indicative of two independent electronic states rather than vibronic satellites. A relatively broad, non-Gaussian shape of these bands suggests the presence of several overlap transitions in the low-energy spectral envelope of the $[Fe(trans\text{-}(1R,2R)\text{-}\mathbf{2})_2](PF_6)_2$ complex, which agrees well with the TDDFT calculations shown below.

For the $[Fe(cis\text{-}\mathbf{2})_2](PF_6)_2$ complex, variable-temperature UV–Vis spectra were conveniently recorded in propionitrile (b.p. = 98 °C) up to 90 °C and showed gradual and significant decrease in peak intensities (Table S5). There were also two isosbestic points observed in the variable-temperature series at ~ 300 and 340 nm (Fig. 5). Potentially, the presence of those points combined with the decrease in band intensities may suggest gradual iron center spin state change from low-spin to high-spin. However, Mössbauer spectra of the $[Fe(cis\text{-}\mathbf{2})_2](PF_6)_2$ complex recorded at 10 K and room temperature (Fig. 5) are clearly indicative that the complex remains in a low-spin state (Table 3). The DFT-predicted Mössbauer parameters [55,56] are listed in Table 3 and are in excellent agreement with the experimental data confirming the low-spin state of the $[Fe(cis\text{-}\mathbf{2})_2](PF_6)_2$ complex. A simplistic explanation of the stability of the low-spin configuration of the $[Fe(cis\text{-}\mathbf{2})_2](PF_6)_2$ and $[Fe(trans\text{-}(1R,2R)\text{-}\mathbf{2})_2](PF_6)_2$ complexes is stabilization of orthogonal $3d_{xz}$ and $3d_{yz}$ orbitals due to backbonding with the π-antibonding orbitals of the orthogonal C═N ligands. This orthogonal configuration of the C═N bonds maximizes the amount of backbonding that can occur and favors the low spin state (Fig. 6).

3.4. Electrochemistry and spectroelectrochemistry

Both compounds possess one reversible oxidation and several overlapping irreversible reduction processes determined by cyclic voltammetry (CV) and differential pulse voltammetry (DPV) experiments (Figs. 7, S49). Oxidation of both isomers under spectroelectrochemical conditions in a MeCN/0.3 M TBAP system at room temperature results in a nearly identical (Fig. 8, S41-S44). In particular, the intensities of the low-energy bands at ~ 600 and ~ 500 nm decrease, while a moderate increase in transition intensities was observed in the 300 – 400 nm region. These changes, along with the lack of NIR transitions that are characteristic for the organic chromophores in a cation-radical state [57,58] suggest that the first oxidation is metal-centered (Fe^{II}/Fe^{III} process), which agrees well with our DFT data. In agreement with the electrochemical data, the first oxidation is reversible under spectroelectrochemical conditions, and the initial starting complexes can be recovered upon reduction of the oxidized species under spectroelectrochemical experiments (Fig. S43). Chemical oxidation of the $[Fe(cis\text{-}\mathbf{2})_2](PF_6)_2$ and $[Fe(trans\text{-}(1R,2R)\text{-}\mathbf{2})_2](PF_6)_2$ complexes results in changes identical to what was observed for the spectroelectrochemical experiments and thus confirm the oxidation of the iron(II) center (Fig. S44).

3.5. DFT and TDDFT calculations

In order to elucidate the electronic structures of the $[Fe(cis\text{-}\mathbf{2})_2](PF_6)_2$ and $[Fe(trans\text{-}(1R,2R)\text{-}\mathbf{2})_2](PF_6)_2$ complexes as well as provide an

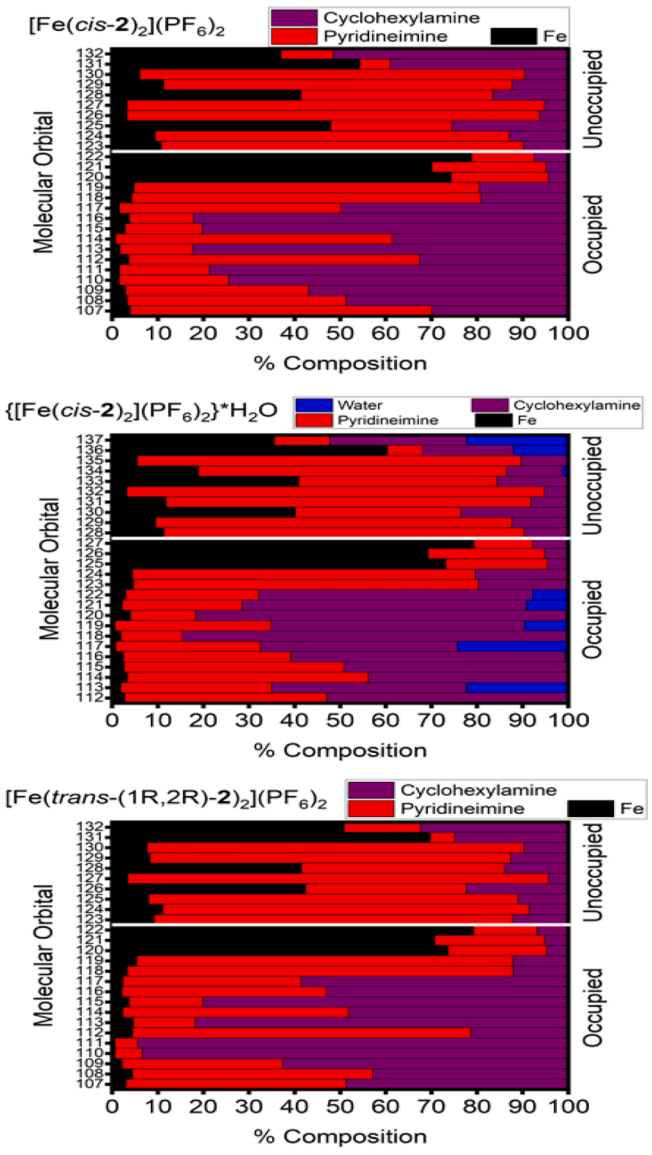

Fig. 12. DFT-predicted MO composition diagrams for $[Fe(\textit{cis}\text{-}\mathbf{2})_2]^{2+}$, $\{[Fe(\textit{cis}\text{-}\mathbf{2})_2]^*H_2O\}^{2+}$, and $[Fe(\textit{trans}\text{-}(1R,2R)\text{-}\mathbf{2})_2]^{2+}$.

insight into the nature of the transitions observed in the UV–Vis spectra of these compounds, we conducted a set of DFT and TDDFT calculations. In addition to the simulated UV–Vis spectra and CD spectra presented in Figs. 9 and S47, the molecular orbital energy-level diagram for $[Fe(\textit{cis}\text{-}\mathbf{2})_2]^{2+}$, $\{[Fe(\textit{cis}\text{-}\mathbf{2})_2]^*H_2O\}^{2+}$, and $[Fe(\textit{trans}\text{-}(1R,2R)\text{-}\mathbf{2})_2]^{2+}$ is shown in Fig. 10; the frontier orbital images are available from Fig. 11 and Figs. S45-S46. The molecular orbital compositions are depicted in Fig. 12. As expected from the experimental UV–Vis spectra, electrochemical, and spectroelectrochemical experiments, the electronic structures of $[Fe(\textit{cis}\text{-}\mathbf{2})_2]^{2+}$ and $[Fe(\textit{trans}\text{-}(1R,2R)\text{-}\mathbf{2})_2]^{2+}$ are nearly identical. Moreover, coordination of the water molecule to $[Fe(\textit{cis}\text{-}\mathbf{2})_2]^{2+}$ does not affect its electronic structure in any significant way (Figs. 10 and 12).

DFT calculations predict that the HOMO – HOMO-2 orbitals in all complexes should be predominantly iron-centered with more than 70 % contribution from the iron ions (Fig. 12). These orbitals have d_{xy}, d_{xz}, and d_{yz} characters as expected for the pseudo-octahedral complexes in low-spin configuration. In contrarily, the LUMO and LUMO + 1 are predominantly ligand-centered orbitals (Figs. 11 and 12). Such an electronic structure creates the possibility for low-energy MLCT transitions. In agreement with this observation, the TDDFT calculations suggest that the UV–Vis spectra of $[Fe(\textit{cis}\text{-}\mathbf{2})_2]^{2+}$ and $[Fe(\textit{trans}\text{-}(1R,2R)\text{-}\mathbf{2})_2]^{2+}$ should be nearly identical. TDDFT calculations predict that the intense, low-energy band observed at ~ 600 nm (predicted at ~ 520 nm) is dominated by HOMO-1, HOMO-2 → LUMO, LUMO + 1 single-electron excitations and several TDDFT-predicted bands in the 400–500 nm region should also have MLCT character. These excited states contribute to the negative signal observed in the CD spectrum of $[Fe(\textit{trans}\text{-}(1R,2R)\text{-}\mathbf{2})_2]^{2+}$ at ~ 500 nm. According to the TDDFT calculations, the most intense band in CD spectrum of $[Fe(\textit{trans}\text{-}(1R,2R)\text{-}\mathbf{2})_2]^{2+}$ should be located around 300 nm, which correlates well with the experimental data. This band is dominated by intra-ligand single-electron transitions and has π-π* character.

In addition, we also calculated total spin densities in oxidized $[Fe(\textit{cis}\text{-}\mathbf{2})_2]^{3+}$ and $[Fe(\textit{trans}\text{-}(1R,2R)\text{-}\mathbf{2})_2]^{3+}$ and reduced $[Fe(\textit{cis}\text{-}\mathbf{2})_2]^{+}$ and $[Fe(\textit{trans}\text{-}(1R,2R)\text{-}\mathbf{2})_2]^{+}$ species (Supporting Information Table S6 and Fig. S48). In agreement with the electronic structure and electrochemical data on $[Fe(\textit{cis}\text{-}\mathbf{2})_2]^{2+}$ and $[Fe(\textit{trans}\text{-}(1R,2R)\text{-}\mathbf{2})_2]^{2+}$ complexes, DFT calculations indicate that the first oxidation is iron-centered and transforms Fe(II) to Fe(III), while the first reduction is ligand-centered process.

4. Conclusion

The facile synthesis of $[Fe(\textit{cis}\text{-}\mathbf{2})_2](PF_6)_2$ or $[Fe(\textit{trans}\text{-}(1R,2R)\text{-}\mathbf{2})_2](PF_6)_2$ from either hydrolysis or self-assembly routes, gives a C_2-symmetrial complex ion of iron(II) bearing two, tridentate mixed imine/amine ligands in a merdional configuration around the iron center. The *cis*-1,2-cyclohexyl backbone is unique in that it provides for the formation of amine to water hydrogen bonds within a cavity created by the cyclohexyl rings. Short metal to N_{imine} bond distances, long C═N bond distances, and a lower frequency C═N stretch frequency suggest metal-to-ligand backbonding stabilizes the complex. Due to this stabilization, the complex is low spin at all temperatures explored from 10 K to 300 K. The *cis*- and *trans*-(1R,2R)-cyclohexane diamine ligand backbone yields a unique coordination sphere with potential applications for host–guest chemistry. Similar studies with other transition metal complexes bearing *cis*-1,2-cyclohexanediamine type ligands are underway which show similar bonding to hydrogen-bond acceptor molecules.

CRediT authorship contribution statement

Carl B. Hollandsworth: Conceptualization, Investigation, Methodology, Project administration, Supervision, Writing – original draft, Writing – review & editing. **Blayne M. Griffin:** Methodology, Investigation. **John Raymon Pruden:** Methodology, Investigation. **Nikolay N. Gerasimchuk:** Formal analysis, Investigation, Methodology, Supervision, Writing – original draft, Writing – review & editing. **Dustin E. Nevonen:** Formal analysis, Investigation, Visualization. **Rachel R. Nickel:** Formal analysis, Methodology, Investigation. **Johan van Lierop:** Formal analysis, Methodology, Investigation. **Victor N. Nemykin:** Formal analysis, Investigation, Methodology, Supervision, Validation, Visualization, Writing – original draft, Writing – review & editing.

Declaration of Competing Interest

The authors declare that they have no known competing financial interests or personal relationships that could have appeared to influence the work reported in this paper.

Data availability

Data will be made available on request.

Acknowledgements

We would like to thank Mrs. Olga Gerasimchuk for help with electronic absorption spectroscopy. CBH would like to acknowledge Dr. David Thomas at Lyon University (Batesville, AR) for use of the Genesys spectrophotometer. CBH also thanks Dr. Patrick Desrochers and Ms. Jamie Freeman at the University of Central Arkansas (Conway, AR) for use of and assistance with their high-field NMR spectrophotometer. CBH thanks Dr. Kevin Stewart at Harding University (Searcy, AR) for use of the ATR IR instrument. NG is grateful to Missouri State University for continuous support of the X-ray diffraction laboratory. VNN would like to acknowledge that funding for this project was provided by NSF grant # CHE-2153081.

Appendix A. Supplementary data

Supplementary data to this article can be found online at https://doi.org/10.1016/j.poly.2023.116669.

References

[1] (a) Fürstner, A. ACS Central Science, 2016 2 (11), 778-789. (b) H. M. Neu, V. V. Zhdankin, V. N. Nemykin, Binuclear iron(III) phthalocyanine(μ-oxodimer)/tetrabutylammonium oxone: a powerful catalytic system for oxidation of hydrocarbons in organic solution Tetr. Lett. 51, (2010) 6545-6548. (c) H. M. Neu, M. S. Yusubov, V. V. Zhdankin, V. N. Nemykin, Binuclear iron(III) phthalocyanine (μ-oxo-dimer)-catalyzed oxygenation of aromatic hydrocarbons with iodosylbenzene sulfate and iodosylbenzene as the oxidants Adv. Synth. Catal. 351, (2009) 3168-3174. (d) I. M. Geraskin, M. W. Luedtke, H. M. Neu, V. N. Nemykin, V. V. Zhdankin, Organic iodine(V) compounds as terminal oxidants in iron(III) phthalocyanine catalyzed oxidation of alcohols Tetr. Lett. 49, (2008), 7410-7412. (e) A. B. Sorokin, Recent progress on exploring μ-oxo bridged binuclear porphyrinoid complexes in catalysis and material science Coord. Chem. Rev. 389, (2019), 141-160.

[2] C.B. Hollandsworth, J.R. Pruden, W. Clark, N. Gerasimchuk, X-ray structural determination and comparison of Bis-imine Schiff bases with trans- and cis-1,2-cyclohexanediamine backbones, J. Mol. Struct. 1255 (2022), 132430.

[3] Y. Zhang, L. Xiang, Q. Wang, X. Duan, E. Bergin, Synthesis, structure, and catalytic activity of chiral Cu(II) and Ag(I) complexes with (S, S)-1,2-diaminocyclohexane-based N4-donor ligands, Inorg. Chim. Acta 361 (5) (2008) 1246–1254.

[4] R. Frauenlob, M.M. McCormack, C.M. Walsh, E. Bergin, Rapid, in situ synthesis of bidentate ligands: chromatography-free generation of catalyst libraries, Org. Biomol. Chem. 9 (2011) 6934–6937.

[5] M. Lashanizadegan, M. Sarkheil, Synthesis, hydrolysis and fluorescence of Schiff base derivatives of (±) trans-1,2-diaminocyclohexane (DACH) in Co(II), Zn(II), Ni (II) and Cu(II) Complexes, Main Group Chem. 12 (2013) 15–23.

[6] T. Kylmala, N. Kuuloja, Y. Xu, K. Rissanen, R. Franzen, Synthesis of Chlorinated Biphenyls by Suzuki Cross-Coupling Using Diamine or Diimine-Palladium Complexes, Eur. J. Org. Chem. 23 (2008) 4019–4024.

[7] a) H. Liu, H.-L. Zhang, S.-J. Wang, A.-Q. Mi, Y.-Z. Jiang, L.-Z. Gong, Discovery of chiral catalysts by asymmetric activation for highly enantioselective diethylzinc addition to imines: using racemic and achiral diimines as effective activators, Tetrahedron: Asymmetry, 16 (2005) 2901–2907. b) Yadong Zhang, Li Xiang, Qiuwen Wang, Xin-Fang Duan, Guofu Zi, Synthesis, structure, and catalytic activity of chiral Cu(II) and Ag(I) complexes with (S,S)-1,2-diaminocyclohexane-based N4-donor ligands, Inorganica Chimica Acta, 361(5) (2008) 1246–1254. c) P. Pallavicini, V. Amendola, Y. D. Fernandez, M. Ghisalberti, L. Linati, C. Mangano, A. M. Lanfredi, C. Massera, Bis-bidentate vs. bis-tridentate imino-heterocycle ligands in the formation of dinuclear helical complexes of Fe(II). Dalton Trans. (2003) 575–580.

[8] Y.L. Bennani, S. Hanessian, trans-1,2-Diaminocyclohexane Derivatives as Chiral Reagents, Scaffolds, and Ligands for Catalysis: Applications in Asymmetric Synthesis and Molecular Recognition, Chem. Rev. 97 (1997) 3161–3196.

[9] F. Piccinelli, A. Speghini, M. Monari, M. Bettinelli, New chiral pyridine-based Eu (III) complexes: Study of the relationship between the nature of the ligands and the 5D0 luminescence spectra, Inorg. Chim. Acta 385 (2012) 65–72.

[10] F. Piccinelli, M. Leonzio, M. Bettinelli, A. Melchior, G. Faura, Luminescent Eu3+ complexes in acetonitrile solution: Anion sensing and effect of water on the speciation, Inorg. Chim. Acta 453 (2016) 751–756.

[11] F. Piccinelli, M. Leonzio, M. Bettinelli, M. Monari, C. Grazioli, A. Melchior, M. Tolazzi, Tuning of the sensing properties of luminescent Eu3+ complexes towards the nitrate anion, Dalton Trans. 8 (2016) 3310–3318.

[12] C.R. Baar, L.P. Carbray, M.C. Jennings, R.J. Puddephatt, Stereoselective Formation of Platinum−Carbon Bonds from Imines, J. Am. Chem. Soc. 122 (2000) 176–177.

[13] G.C. Van Stein, G. van Koten, K. Vrieze, C. Brevard, A.L. Spek, Structural investigations of silver(I) and copper(I) complexes with neutral nitrogen (N4) donor ligands: x-ray crystal and molecular structure of the dimer [Ag2{.mu.-(R)(S)-1,2-(py-2-CH:N)2Cy}2](O3SCF3)2 and proton, carbon-13, and INEPT silver-109 and nitrogen-15 NMR solution studies, J. Am. Chem. Soc. 106 (1984) 4486–4492.

[14] S. Oshima, N. Hirayama, K. Kubono, H. Kokusen, T. Honjo, Ion-pair extraction behavior of divalent metal cations using neutral di-Schiff base ligands derived from 1,2-cyclohexanediamine and o-phenylenediamine, Talanta 59 (2003) 867–874.

[15] M. Lashanizadegan, M. Sarkheil, Solvent-dependent synthesis and mono-hydrolysis of the di-Schiff base of (±)trans-1,2-cyclohexanediamine and 2-pyridinecarboxaldehyde in Cu(II), Co(II) and Zn(II) complexes, J. Serb. Chem. Soc. 77 (11) (2012) 1589.

[16] P. Krumholtz, Studies on the Coordinate Bond. VI. The Nature of the Chromophoric Group in Iron(II) Complexes of Tridentate Imine Ligands, Inorg. Chem. 5 (1965) 612–616.

[17] S. Kano, H. Nakano, M. Kojima, N. Baba, K. Nakajima, An effect of the ionic radii of lanthanide(III) ions on the structure and catalytic properties of chiral Schiff base-lanthanide(III) complexes, Inorg. Chim. Acta 349 (2003) 6.

[18] A.A. El-Samahy, E.-E.-A. Abu-Gharib, A.-E. Eltaher, R.M. El-Khatib, J. Burgess, Solvent effects on reactivity trends for base hydrolysis of iron(II) complexes of tridentate Schiff base imine ligands, Trans. Met. Chem. 17 (1992) 438–442.

[19] G.S. Girolami, A Guide to Using the SHELXTL Crystallographic Software Package, University of Illinois at Urbana-Champaign, Department of Chemistry, 2004.

[20] R.H. Blessing, Absorption correction: multi-scan method, Acta Cryst. A. 51 (1995).

[21] George Sheldrick in Bruker APEX2 and APEX3 Software Suits; Bruker AXS, Inc. Madison, WI. USA.

[22] L.J. Farrugia, ORTEP-3 for Windows - a version of ORTEP-III with a Graphical User Interface (GUI), J. Appl. Cryst. 30 (1997) 565.

[23] M.N. Burnett, C.K. Johnson, ORTEP-III: Oak Ridge Thermal Ellipsoid Plot Program for Crystal Structure Illustrations, Oak Ridge National Laboratory, Oak Ridge, TN, USA, 1996.

[24] Mercury Software, CCDC (Cambridge Crystal Data Centre, Cambridge), England, 4.2 ed., 2016.

[25] Gaussian 16, Revision B.01, Frisch, M. J.; Trucks, G. W.; Schlegel, H. B.; Scuseria, G. E.; Robb, M. A.; Cheeseman, J. R.; Scalmani, G.; Barone, V.; Petersson, G. A.; Nakatsuji, H.; Li, X.; Caricato, M.; Marenich, A. V.; Bloino, J.; Janesko, B. G.; Gomperts, R.; Mennucci, B.; Hratchian, H. P.; Ortiz, J. V.; Izmaylov, A. F.; Sonnenberg, J. L.; Williams-Young, D.; Ding, F.; Lipparini, F.; Egidi, F.; Goings, J.; Peng, B.; Petrone, A.; Henderson, T.; Ranasinghe, D.; Zakrzewski, V. G.; Gao, J.; Rega, N.; Zheng, G.; Liang, W.; Hada, M.; Ehara, M.; Toyota, K.; Fukuda, R.; Hasegawa, J.; Ishida, M.; Nakajima, T.; Honda, Y.; Kitao, O.; Nakai, H.; Vreven, T.; Throssell, K.; Montgomery, J. A., Jr.; Peralta, J. E.; Ogliaro, F.; Bearpark, M. J.; Heyd, J. J.; Brothers, E. N.; Kudin, K. N.; Staroverov, V. N.; Keith, T. A.; Kobayashi, R.; Normand, J.; Raghavachari, K.; Rendell, A. P.; Burant, J. C.; Iyengar, S. S.; Tomasi, J.; Cossi, M.; Millam, J. M.; Klene, M.; Adamo, C.; Cammi, R.; Ochterski, J. W.; Martin, R. L.; Morokuma, K.; Farkas, O.; Foresman, J. B.; Fox, D. J. Gaussian, Inc., Wallingford CT, 2016.

[26] A.D. Becke, Density-functional exchange-energy approximation with correct asymptotic behaviour, Phys. Rev. A 38 (1988) 3098–3100.

[27] J.P. Perdew, Density-functional approximation for the correlation energy of the inhomogeneous electron gas, Phys. Rev. B 33 (1986) 8822–8824.

[28] A.J.H. Wachters, Gaussian Basis Set for Molecular Wavefunctions Containing Third-Row Atoms, J. Chem. Phys. 52 (1970) 1033–1036.

[29] A.D. McLean, G.S. Chandler, Contracted Gaussian basis sets for molecular calculations. 1. Second row atoms, Z = 11–18, J. Chem. Phys. 72 (1980) 5639–5648.

[30] J.P. Perdew, A. Ruzsinszky, G.I. Csonka, L.A. Constantin, J. Sun, Workhorse semilocal density functional for condensed matter physics and quantum chemistry, Phys. Rev. Lett. 103 (2009) 026403/1–026403/5.

[31] J.P. Perdew, A. Ruzsinszky, G.I. Csonka, L.A. Constantin, S.J. Erratum, Workhorse semilocal density functional for condensed matter physics and quantum chemistry, Phys. Rev. Lett. 103 (2009) 179902/1.

[32] A.D. Becke, Density-functional thermochemistry. III. The role of exact exchange, J. Chem. Phys. 98 (1993) 5648–5652.

[33] P. Hohenberg, W. Kohn, Inhomogeneous electron gas, Phys. Rev. 136 (1964) B864–B871.

[34] W. Kohn, L.J. Sham, Self-consistent equations including exchange and correlation effects, Phys. Rev. 140 (1965) A1133–A1138.

[35] J.C. Slater, The Self-Consistent Field for Molecular and Solids, Quantum Theory of Molecular and Solids, Vol. 4., McGraw-Hill, New York, 1974.

[36] R. Peverati, D.G. Truhlar, M11-L: A local density functional that provides improved accuracy for electronic structure calculations in chemistry and physics, J. Phys. Chem. Lett. 3 (2011) 117–124.

[37] H.S. Yu, X. He, D.G. Truhlar, MN15-L: A new local exchange-correlation functional for Kohn-Sham density functional theory with broad accuracy for atoms, molecules, and solids, J. Chem. Theory Comput. 12 (2016) 1280–1293.

[38] A.J. Cohen, N.C. Handy, Dynamic correlation, Mol. Phys. 99 (2001) 607–615.

[39] N.C. Handy, A.J. Cohen, Left-right correlation energy, Mol. Phys. 99 (2001) 403–412.

[40] J.P. Perdew, K. Burke, M. Ernzerhof, Generalized gradient approximation made simple, Phys. Rev. Lett. 77 (1996) 3865–3868.

[41] J.P. Perdew, K. Burke, M. Ernzerhof, Errata: Generalized gradient approximation made simple, Phys. Rev. Lett. 78 (1997) 1396.

[42] R. Peverati, Y. Zhao, D.G. Truhlar, Generalized gradient approximation that recovers the second-order density-gradient expansion with optimized across-the-board performance, J. Phys. Chem. Lett. 2 (2011) 1991–1997.

[43] O. Gunnarsson, B.I. Lundqvist, Exchange and correlation in atoms, molecules, and solids by the spin-density-functional formalism, Phys. Rev. B 13 (1976) 4274–4298.

[44] A.D. Boese, N.C. Handy, New exchange-correlation density functionals: The role of the kinetic-energy density, J. Chem. Phys. 116 (2002) 9559–9569.

[45] J.M. Tao, J.P. Perdew, V.N. Staroverov, G.E. Scuseria, Climbing the density functional ladder: Nonempirical meta-generalized gradient approximation designed for molecules and solids, Phys. Rev. Lett. 91 (2003) 146401/1–146401/4.
[46] V.N. Staroverov, G.N. Scuseria, J. Tao, J.P. Perdew, Comparative assessment of a new nonempirical density functional: Molecules and hydrogen-bonded complexes, J. Chem. Phys. 119 (2003) 12129–12137.
[47] T.V. Voorhis, G.E. Scuseria, A novel form for the exchange-correlation energy functional, J. Chem. Phys. 109 (1998) 400–410.
[48] J.D. Chai, M. Head-Gordon, Long-range corrected hybrid density functionals with damped atom-atom dispersion corrections, PCCP 10 (2008) 6615–6620.
[49] D.E. Nevonen, L.S. Ferch, B.R. Schrage, V.N. Nemykin, Charge-Transfer Spectroscopy of Bisaxially Coordinated Iron(II) Phthalocyanines through the Prism of the Lever's EL Parameters Scale, MCD Spectroscopy, and TDDFT Calculations, Inorg. Chem. 61 (2022) 8250–8266.
[50] B.R. Schrage, W. Zhou, L.A. Harrison, D.E. Nevonen, J.R. Thompson, K.E. Prosser, C.J. Walsby, C.J. Ziegler, D.B. Leznoff, V.N. Nemykin, Resolving a Half-Century-Long Controversy between (Magneto)optical and EPR Spectra of Single-Electron-Reduced [PcFe]-, [PcFeL]-, and [PcFeX]2- Complexes: Story of a Double Flip, Inorg. Chem. 61 (2022) 20177–20199.
[51] J. Tomasi, B. Mennucci, R. Cammi, Quantum mechanical continuum solvation models, Chem. Rev. 105 (2005) 2999–3093.
[52] Tenderholt, A. L. QMForge, version 2.1; Standord University: Stanford, CA, 2011. https://qmforge.net/.
[53] P. Murphy, S.J. Dalgarno, M.J. Paterson, Chem. A Eur. J. 120 (5) (2016) 824–839.
[54] T. Steiner, Angew. Chem. Int. Ed. 41 (2002) 48–76.
[55] V.N. Nemykin, K. Nagao, V.Y. Chernii, V.K. Belsky, Mössbauer, Crystallographic, and Density Functional Theoretical Investigation of the Electronic Structure of Bis-Ligated Low-Spin Iron(II) Phthalocyanines, Eur. J. Inorg. Chem. 2001 (2001) 733–743.
[56] V.N. Nemykin, D.E. Nevonen, L.S. Ferch, M. Shepit, D.E. Herbert, J. van Lierop, Accurate Prediction of Mössbauer Hyperfine Parameters in Bis-Axially Coordinated Iron(II) Phthalocyanines Using Density Functional Theory Calculations: A Story of a Single Orbital Revealed by Natural Bond Orbital Analysis, Inorg. Chem. 60 (2021) 3690–3706.
[57] E.A. Makarova, Y.V. Zatsikha, K.M.E. Newman, V.K. Paidi, V.A. Beletsky, J. van Lierop, E.A. Lukyanets, V.N. Nemykin, Direct Synthesis of an Unprecedented Stable Radical of Nickel(II) 3,5-Bis(dimedonyl)azadiisoindomethene with Strong and Narrow Near-Infrared Absorption at $\lambda \sim 1000$ nm, Inorg. Chem. 56 (11) (2017) 6052–6055.
[58] D.E. Nevonen, G.T. Rohde, V.N. Nemykin, New Insight into an Old Problem: Analysis, Interpretation, and Theoretical Modeling of the Absorption and Magnetic Circular Dichroism Spectra of Monomeric and Dimeric Zinc Phthalocyanine Cation Radical, Inorg. Chem. 58 (2019) 14120–14135.